Industry Implementation of Mathematical Models: Examples in Steel Processing

This paper was originally presented as the Howe Memorial Lecture at AISTech 2009 in St. Louis, Mo.

Mathematical process models — including fully online, semi-online, offline and literature models — can induce beneficial changes to process operation. Examples are taken from the author's experience in modeling the continuous casting of steel and related processes.

Henry Marion Howe was one of the first to apply modern scientific methods to improve understanding of the art of steelmaking. After spending hours carefully observing details of plant operation, he was not afraid to express controversial opinions, and he created ideas that had practical impact on real steelmaking and casting processes. In the same spirit as Howe's thought-provoking landmark paper in 1875 entitled "What Is Steel?"[1] this paper asks the questions: "What is a model?", "What is model implementation?", and "Why model?" and offers opinions based on examples taken from the author's experience in modeling the continuous casting of steel and related processes.

What Is a Model?

A model is a set of mathematical equations and constants which takes input data and outputs quantitative predictions that can be tested with observations in the real world, as shown in Figure 1.

Figure 1

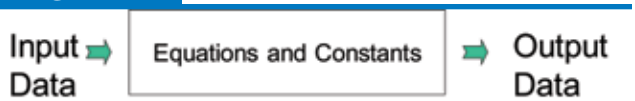

Definition of a process model.

Kepler's Law — Taking an example from Howe's era before computers, Kepler's third law of planetary motion from 1619 is a model that takes, as input, the distance of a planet from the sun, and outputs its orbital period (or year):

$$P = R^{3/2} \quad \text{(Eq. 1)}$$

where

P = orbital period (Earth years) and
R = distance from Sun (Earth orbital radii).

After calibrating this equation by choosing units to match Earth's year, this model can predict the year of any planet or object orbiting in our solar system. Taking Mars, for example: inputting R = 1.52 gives P = 1.88 Earth years. These predictions match very well with astronomical measurements. In fact, its accuracy is taken so much for granted that published predictions from this model are accepted as fact. Note, however, that its prediction for Pluto of 248 Earth years has never been measured, as it has traveled less than one-third of an orbit since its discovery in 1930.

Shell Growth Equation — It is important to emphasize that a model includes both the equation and its constants. Taking an example of a process model closer to steelmaking, the shell growth equation is given as:

$$s = k\sqrt{t} \quad \text{(Eq. 2)}$$

where

s = shell thickness (in.),
k = solidification constant (~1 in.-min$^{-0.5}$) and
t = time below meniscus (min) = distance below meniscus (in.)/casting speed (in./min).

This simple but powerful equation is the foundation of caster design. It is commonly used to find the maximum casting speed to avoid letting the molten core extend beyond the metallurgical length, or final solidification point. Although it is reasonable for simple design

Author

Brian G. Thomas, Mechanical Science and Engineering, University of Illinois at Urbana-Champaign, Urbana, Ill. (bgthomas@illinois.edu)

purposes, the solidification constant k varies somewhat with casting conditions, such as spray cooling rate. It is important to note that the accuracy of this model depends on finding a good value for k. Furthermore, a different value of k is needed to predict shell thickness at mold exit than to predict metallurgical length. A k fit to one caster might not be accurate somewhere else. Thus, empirical constants, such as k, can be used only with the original equation and conditions used to find them.

Types of Models — Models can be classified in several ways. First, every model falls in a spectrum between fundamental and empirical. Fundamental models, such as Kepler's law, are solutions of mechanistic equations based on accepted theory, and so can be extended reliably to far beyond their proven range. At the other extreme, empirical models are curve-fits of measured data, which are accurate only over the limited range of input conditions where they have been calibrated with measurements. Although it does have a theoretical basis, the shell growth equation is an example of a mainly empirical model.

Second, models can be classified according to the complexity of their solution method. Analytical solutions, such as the two examples given above, are closed-form solutions of mathematical equations which make it easy to evaluate and see trends. Computational models solve complex systems of differential equations by discretizing them into small regions where simple approximations can be made. They are based on mechanistic natural laws which (hopefully) govern the phenomena of interest. These laws include the equations governing the conservation and transport of mass, momentum, mechanical force, electromagnetic force and energy, in addition to thermodynamics, phase equilibria, kinetics and other relations. Experimental data are incorporated in their most fundamental form, through the material properties. Note that general-purpose software packages are not models, but they serve as useful frameworks for model development by providing tools for solving the equations. By definition, models require a combination of mathematics and experimental measurements. Owing to the tremendous complexity of real processes, only a tiny fraction of the relevant phenomena can be modeled at one time. Thus, the accuracy of the best computational models will always be limited by the power of available computers.

Finally, models can be classified according to how they are implemented to benefit industrial practice.

Figure 2

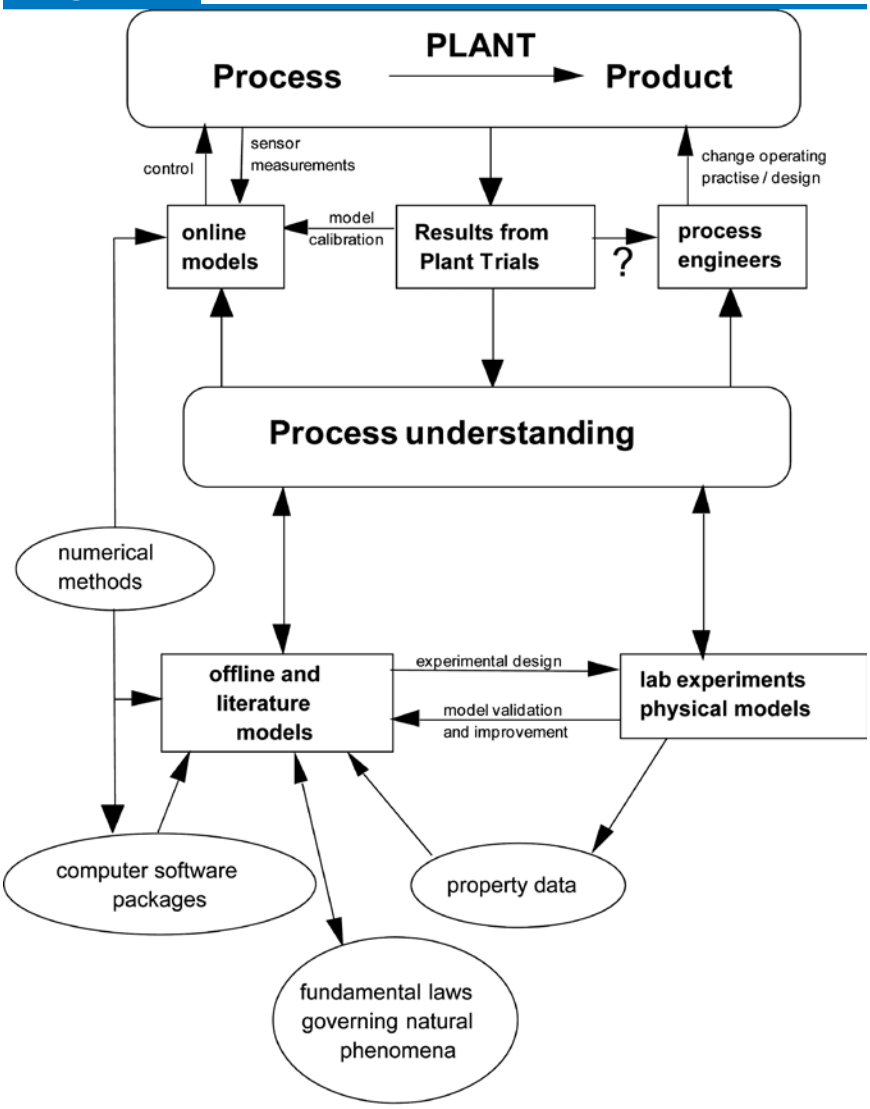

Flow chart for the implementation of process models in industry.[2]

What Is Model Implementation?

Mathematical process models can be applied in many different ways to serve industry by inducing beneficial changes to process operations, which Figure 2 aims to illustrate. The aim of industry is to make a profit by processing products. Two ways to help the steel industry do this are to improve product quality and to reduce production costs. Thus, a reasonable modeling objective is to minimize some defect by specifying achievable changes to individual processes. The model has not been implemented until this tangible change has taken place in the plant.

Changes can be classified according to the variables affected and the time needed to change them. "Design variables" are difficult to change, and the target audience is usually the builder of the plant or vessel. Standard operating practice, or "SOP" variables, refer to the setpoints of process variables that are relatively easy to change in an existing process. "Control variables" change rapidly with time to accommodate variations in input conditions (both accidental and intentional).

The different paths to model implementation have different model requirements. Literature models and offline models create new understanding, and are implemented when process engineers make the changes. Semi-online and online models implement change directly by running at the plant.

Literature Models — The traditional method to effect beneficial changes in plant operation is for process engineers to gain knowledge from previous literature, and to specify changes to SOP. Much of that literature may report results from computational models, or "literature models." Literature models can apply the most sophisticated computational simulations of coupled phenomena in three dimensions, as they can afford the luxury of long computing times. Because the modeler never contacts the process directly, the understanding must be imparted through clear presentation. To be effective, the results of parametric studies must be presented in graphical form, or as a simple curve-fit equation, regardless of whether they originate from models or experiments. To enable implementation, the best graphs plot "something you care about" on the y-axis as a function of "something you can control" on the x-axis. With online publications, video animations add another valuable dimension of insight to the communication of literature model results.

Offline Models — Offline models are used by process engineers, designers, researchers and others in the plant to gain personal insights and understanding about a process. Model results are implemented according to the user's personal knowledge, obtained from all sources, including the plant, pilot plant, physical model, laboratory experiments and previous literature. Decisions should be rooted in process understanding in order to avoid expensive trial and error that can result from plant experiments alone (see the question mark in Figure 2). Like literature models, offline models must be fundamentally based and quantitative in order to accurately explore new conditions. Numerical experiments with a user-friendly offline model are a powerful tool to optimize a particular operation.

Semi-Online Models — A semi-online model typically runs on a stand-alone computer at the operator's desk. The operator uses it as an on-the-spot decision-making tool; it is used to make process changes with the aid of human judgment. Typical examples in steelmaking include determining the optimum amounts of each alloy addition to charge to a furnace or ladle, or when to tap a heat. In continuous casting, an accurate semi-online solidification model can serve as a tool to help the operator troubleshoot the cause of a cracking problem. The start of an internal crack might indicate the location down the caster of a misaligned roll or spray nozzle that was responsible.

Fully Online Models — Fully online models represent the pinnacle of model implementation, as the model resides in the plant computer-control system and implements change on a continuous basis. Input data comes directly from the system, which has access to the relevant real-time sensor signals. Examples in continuous casting include level control systems and breakout detection systems. These models must be extremely fast (to run in real time) and robust (to produce reasonable output for any input condition, including signals from bad sensors). These needs traditionally require a model that is extremely simple, consisting of only a few basic equations and logic statements. Accurate results are needed over only a limited range of operating conditions, so fast empirical models are well-suited to online applications.

Background

Early Process Models — The first "computers" were rooms full of humans doing hand calculations and passing notes. Models using digital computers have their roots in finite element analysis for the aerospace industry in the 1950s, and pioneered by Zienkiewicz.[3] They were adopted into other fields, including steel processing, during the 1960s and 1970s, and have been growing exponentially ever since. Those responsible are too numerous to mention here, and include many previous Howe lecturers. Julian Szekely is noteworthy as the most prolific early modeler, who demonstrated the first heat transfer and computational fluid dynamics models of many different steel processes. While foreshadowing the wide range of applications common today, these early attempts suffered from computer limitations. Mizikar[4] and Brimacombe[5] pioneered the first finite-difference models of shell solidification. These models solve the following transient heat conduction equation, subject to carefully chosen boundary conditions, by following a transverse slice though the shell as it travels downward at the casting speed (Figure 3).

Figure 3

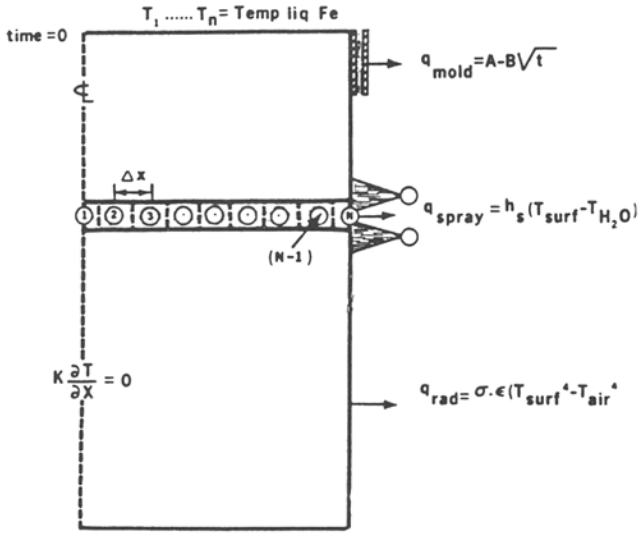

Schematic of continuous cast steel strand, showing 1-D slice domain and boundary conditions.[5]

$$\rho \frac{\partial H}{\partial t} = \nabla \cdot k \nabla T \qquad \text{(Eq. 3)}$$

where

ρ = density (kg/m^3),
H = enthalpy (J/m^3),
t = time (s),
k = thermal conductivity and
T = temperature (°C).

Figure 4 shows typical results[6] from such a model, with shell growth profile on the left and surface temperature on the right. Brimacombe championed the crucial knowledge-creation practice of combining experiments and models together: forcing the models to match reality through calibration and validation. For example, Figure 4 also includes a simulation[6] (line A) to compare with an analytical solution[7] using the integral profile method (line C). More significantly, this figure also contains data points to compare the predictions (line B) with shell thickness measurements (points). The pioneering spirit for model validation in these early days is perhaps best epitomized by how these measurements were obtained: by injecting radioactive gold tracer into the mold of an operating steel caster. After validation, this particular model[8] is more accurate than Equation 2 and was applied with success to predict the following:

- Shell thickness at mold exit.
- Metallurgical length of the caster.
- The location down the caster where cracks initiate.
- Cooling practice below the mold to avoid reheating cracks.

Models such as this one showed that computations are not simply academic curiosities, but can serve as powerful tools to solve practical problems in the real process. Today, it is standard practice for all models to be tested rigorously, first using analytical solutions (to validate the internal consistency of the model and mesh refinement), and then with measurements from experiments or plant trials (to validate modeling assumptions, property data and boundary conditions). This methodology is the foundation of modern computational modeling.

The Computer Revolution — Advances in the silicon chip and user-friendly software have fundamentally transformed the approach to process analysis and enabled great leaps in the capabilities of mathematical process models. As powerful computers now pervade almost every aspect of modern life, it is easy to forget how difficult computational modeling was in the early days, when Brimacombe and his colleagues were writing the first finite-difference models of continuous casting. After writing a program, it had to be typed onto punch cards, carried over to the computer building, and given to the computer operator. A simple compiler error would not be spotted until the results were collected the next day. A calculation that would today take only a few minutes on a personal computer might have been terminated by the mainframe operator before finishing, while burning up an entire year's computing allocation. Achieving meaningful results with these primitive tools makes the early modeling accomplishments all the more impressive.

The increase in application of models to steel processing has coincided with tremendous increases in computing power. In the four decades since those first models, computer processor speed has increased more than 100,000-fold, with similar increases in storage capacity and dramatic decreases in cost. This has enabled the size and complexity of casting models to double every 1.5 years.[9] Today, new software is unleashing the potential of pixel-based graphics processing units (GPUs) to perform low-cost, massively parallel calculations, which could speed up computational fluid dynamics codes by 10-fold.[10] The mind-boggling magnitude of these advances can be illustrated by considering the impact that similar advances would have had on the auto industry. If car manufacturing had increased speed, capacity and cost-efficiency to the same extent as computers have, then today's cars should carry more than 200,000 passengers, travel well over 1 million miles per hour, and cost less than $1 to buy. Our increasingly powerful computers allow modeling to play an increasing role in advances to steel process technology.

Figure 4

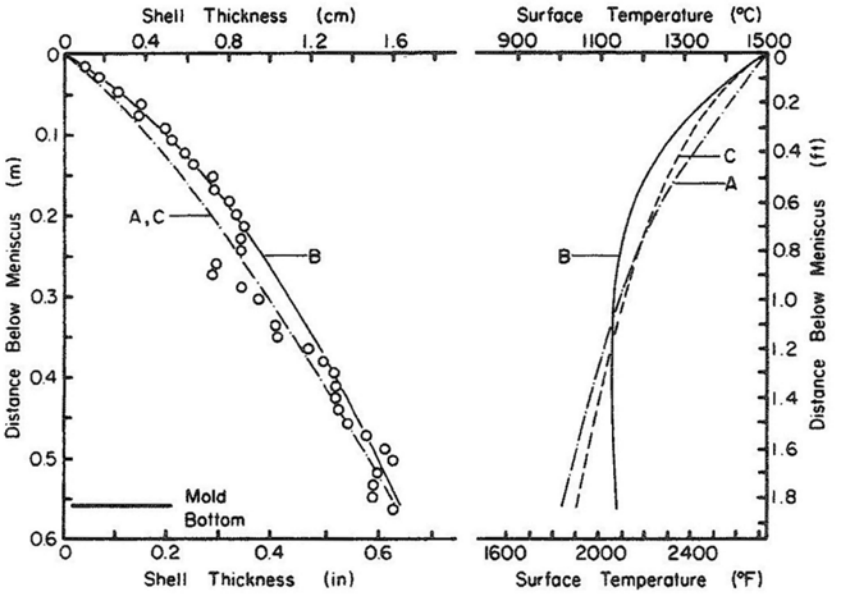

Liquid pool and surface temperature profiles in the mold, comparing finite difference model (A) with analytical solution (C), and finite difference model (B) with shell thickness measured near a beam blank web.[6]

Why Model?

There are many different reasons to develop a process model. These include:

- Increase fundamental understanding of a complex process and its governing phenomena.
- Technology transfer.

Figure 5

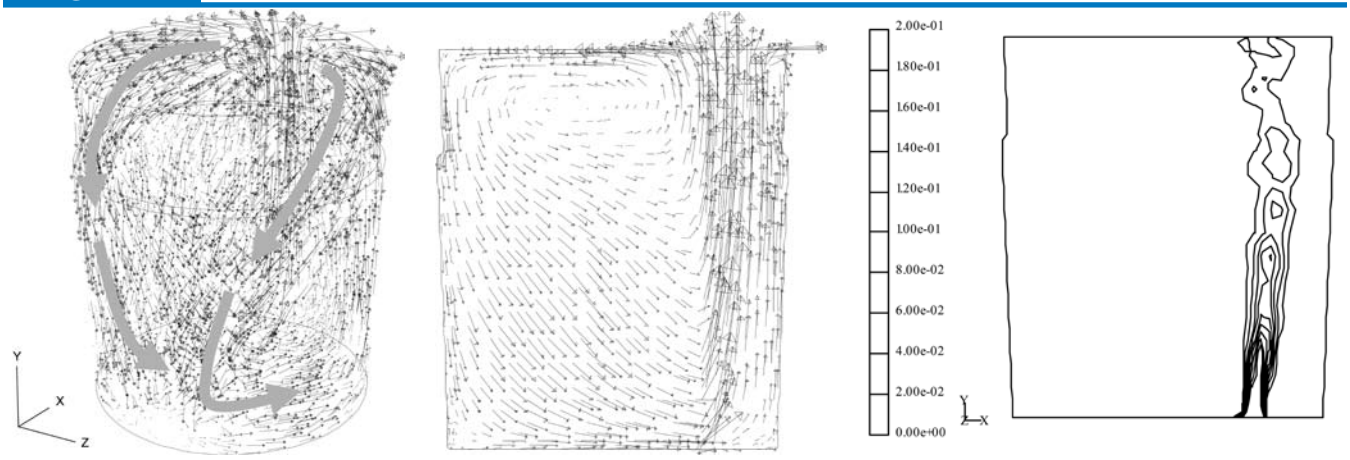

Calculated time-averaged flow field and bubble distribution.[17]

- Design of experiments.
- Evaluation of alternative designs.
- Process optimization.
- Extension and evaluation of plant results.
- Extending lab measurements to quantify properties.
- Assist in scale-up.
- Online process control.

If a clear reason to develop a model cannot be found, then it should not be developed!

Understanding Complex Process Phenomena

Models can be excellent educational tools. The insights gained from careful evaluation of computational model simulations, visualized with 3-D graphics tools that clearly illustrate complex phenomena, often are impossible to obtain in any other way. Even the act of modeling can produce mental discipline in process analysis and deepen understanding of the phenomena which govern it. With increased process understanding, a process engineer can make better decisions and implement improvements to processes.

Ladle Refining — Consider, for example, the ladle refining process. Alloying additions must melt, dissolve and mix into the bulk flow. Additions for deoxidation involve even more complex phenomena, as they also react to create inclusion particles, collide with larger particles and with bubbles, which must be transported through the turbulent fluid to the slag/metal interface, where the impurities are hopefully absorbed and removed. These phenomena all depend on the turbulent flow field, which in turn is governed by jet buoyancy controlled by the gas injection rate. Modeling methods and insights into these phenomena have benefited from decades of contributions from many previous computational modelers of ladle flow, including Emi,[11] Irons,[12] Johansen,[13] Oeters,[14] Guthrie[15] and many others.[16]

Figure 5 shows the flow pattern and gas bubble distribution computed in a 3.6-m-high x 2.7-m-diameter ladle filled with 110 tonnes of steel, and argon gas injected at 0.17 Nm^3/min. through an off-centered porous plug located 0.72 m from centerline.[17] The 3-D computational flow model solves the mass transport (continuity) and momentum balance equations in the molten steel, coupled with the k-ε model for turbulence and a discrete-phase model for the bubbles, and solved in FLUENT.[17] The chaotic effect of turbulent flow on the bubble trajectories was incorporated using the random walk method. The effect of bubble shape (ranging from eccentric ellipsoids to spherical caps) was included using special functions for the drag coefficients.

The results show that the jet of bubbles from the porous plug forms a plume that expands as it rises. The model predicts about 1,700 bubbles (28.2 mm average diameter) in the ladle under pseudo-steady-state conditions, with an average dwell time of 3.4 seconds. The maximum plume velocity of ~0.8 m/second matches previous work. The plume splits into two main streams that swirl diagonally across the top surface, flow down the far side, and converge toward the bottom corner on the opposite side of the porous plug. The returning flow pushes the plume toward the right wall, which can also be seen in the gas concentrations.

After adding 1.82 tonnes of SiMn ferroalloy, over 37 seconds, to the eye that formed directly above the plume, steel samples were collected at a carefully measured location near the top just outside the plume. Equilibrium concentrations were calculated based on the steel, slag and alloy compositions, and the temperature.[18] Model simulations of the concentration changes are shown in Figure 6, based on a two-stage model for alloy dissolution. At first, a layer of solid steel was assumed to freeze around each ferroalloy particle in the size distribution. Although this causes their density to increase, these composite particles are carried mainly across the top of the ladle, while the steel layer grows and then melts. Superheat is important, owing to its effect on this melting time. The low-freezing-temperature alloy trapped inside is assumed to melt before its surrounding shell melts away, so the liquid is released suddenly from a region near the top left edge at the steel-slag interface. This finding explains why Mn recoveries, which varied from 91 to 97%, correlated strongly with the oxygen potential of the slag.

The computed concentration histories in Figure 7 match the behavior of the plant measurements, including its oscillating nature. Variations are likely caused by

Figure 6

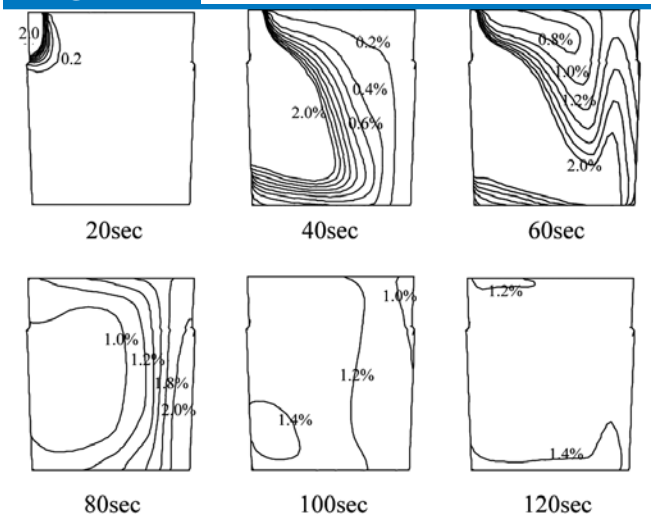

Mixing concentration predicted in center plane (time after start of ferroalloy addition).[17]

Figure 7

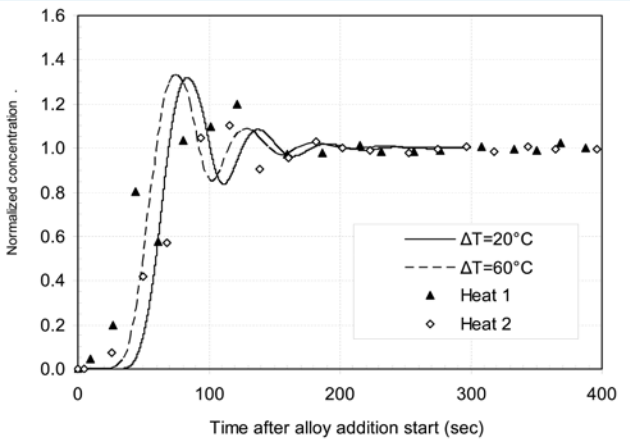

Computed concentration profiles at the sampling point compared with plant measurements.[17]

differences between heats, turbulent fluctuations, and sampling. Note that both the predictions and measurements show an initial concentration peak that exceeds 100% well before mixing is complete. This is due to a local region of solute-rich fluid that circulates around the ladle. Thus, it is not appropriate to define mixing by the time to reach a given percentage of the final concentration. A better definition of mixing time is when the normalized concentration stops varying outside of a range such as 95–105%. It is also important to carefully choose the sampling point and to examine the entire mixing curve.

Using overall mass balance calculations, slag layer weight gain and composition changes are also calculated and agree with measurements. Another practical finding from such models is that an off-center plug location tends to decrease mixing times relative to a centered plug. Empowered by the process understanding provided by models such as this one, plant engineers can create and implement improvements to the process.

Extending Plant Measurements

Fundamentally based offline computational models can be used in the interpretation of plant experiments. In particular, they can be used to extract more fundamental properties from the raw measured quantities. A common example in steel processing is the extraction of heat transfer coefficients and heat flux curves from the temperature measurements of thermocouples. These heat fluxes enable more meaningful comparison between experimental results, because they are less specific to a particular experimental setup.

Nail Board Dip Test — Another example is the measurement of flow conditions near the surface of the continuous slab-casting mold. Steel quality is greatly affected by

Figure 8

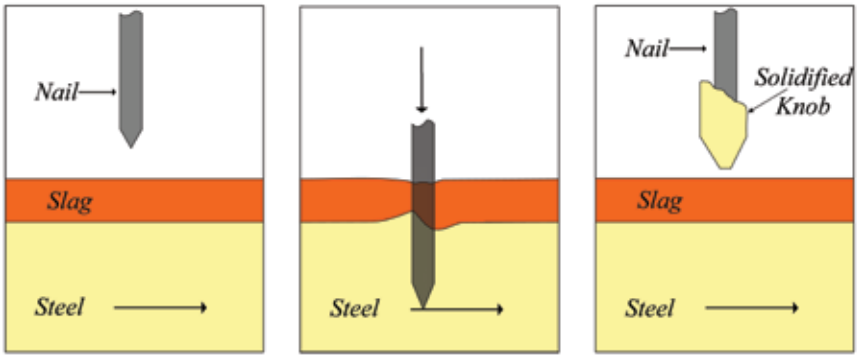

Step 1: Insert nail through slag layer into liquid pool.

Step 2: Hold nail in steel for short time (3–5 s).

Step 3: Remove nail, and measure shape of knob.

Nail board method to measure steel surface speed and direction.

Figure 9

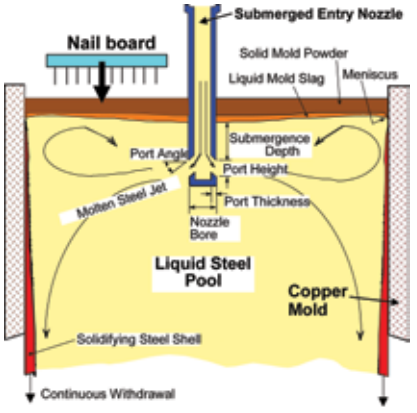

Continuous casting mold showing steel flow, top surface slag layers, and location of nail board insertion.[1]

Figure 10

Flow past immersed column in water model.

Figure 11

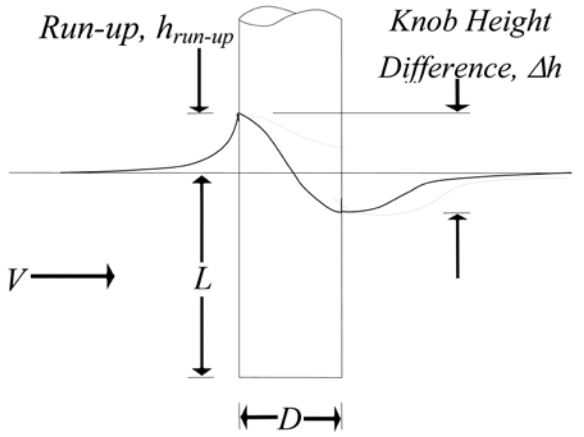

Schematic of flow variables: run-up height and measured knob height difference.

Figure 12

Nail photo showing measurement of solidified knob.

the fluid flow pattern in the mold, which is difficult to measure, owing to the harsh environment and electrical interference. The nail board dip test is a simple yet powerful tool to characterize flow conditions near the top surface. A row of nails is inserted into a long board and dipped perpendicularly through the slag/steel inter-surface for 3–5 seconds, as shown in Figure 8. Upon removal, a knob of steel has solidified on the end of each nail.

Nail board measurements are commonly used to find the depth of the molten slag layer.[19] This is found by affixing an aluminum wire alongside the nails prior to dipping, and recording the difference between the melted wire height and the solidified knob. The profile of the knob heights together indicate the shape of the steel meniscus. The profile is higher near the narrow face for double-roll flow patterns, due to the uplifting effect of flow up the narrow face, as pictured in Figure 9.

The angular profile of the knob can be further analyzed to quantify the surface velocity profile. The high end of the angular profile indicates the direction of steel flow past the nail, as shown in Figures 10–12. Recently, Rietow used a carefully validated computational model to determine a relation to correlate knob height difference, Δh, and nail diameter to surface velocity of the molten steel across the top of the mold.[20] Knob height difference is the difference in height between the low end and the high end of the knob profile at the nail, as shown in Figure 11. The model features 3-D turbulent flow in the steel, coupled with laminar flow in the slag layer, and two free-surface computations using the SPINES method in the finite element CFD package, FIDAP.[21] An example of the model predictions showing the knob shape is given in Figure 13, where the molten steel is flowing from the lower left. The calculated knob height difference varies with the nail diameter, D, the fluid densities, viscosity and interfacial tension, so the interface between molten steel and the slag layer is much different than in a water model.

A compilation of the model results, illustrated in Figure 14, enables accurate, fast measurement of meniscus velocity in a plant setting. The height difference

Figure 13

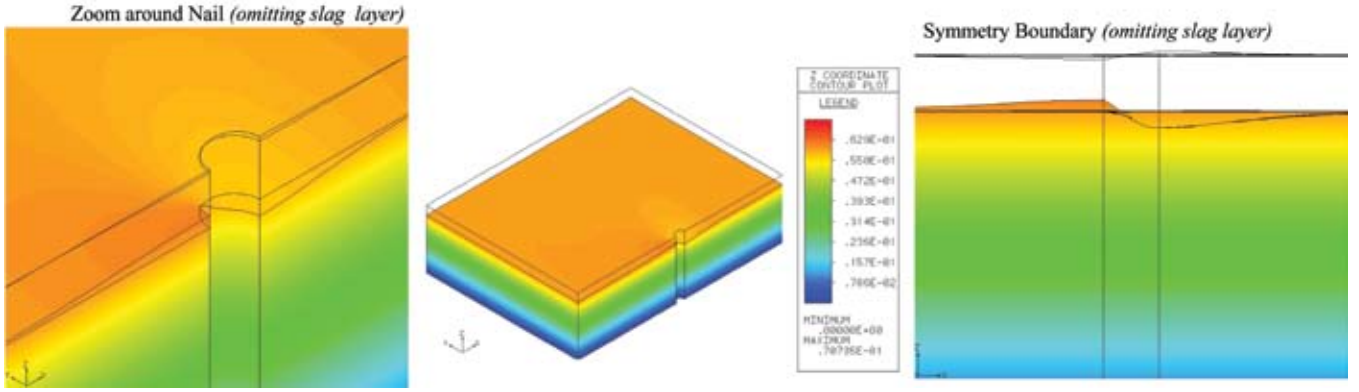

Model of slag/steel interface shape and vertical (z) velocity contours: three views (0.3 m/s; 10-mm-diameter nail).

Figure 14

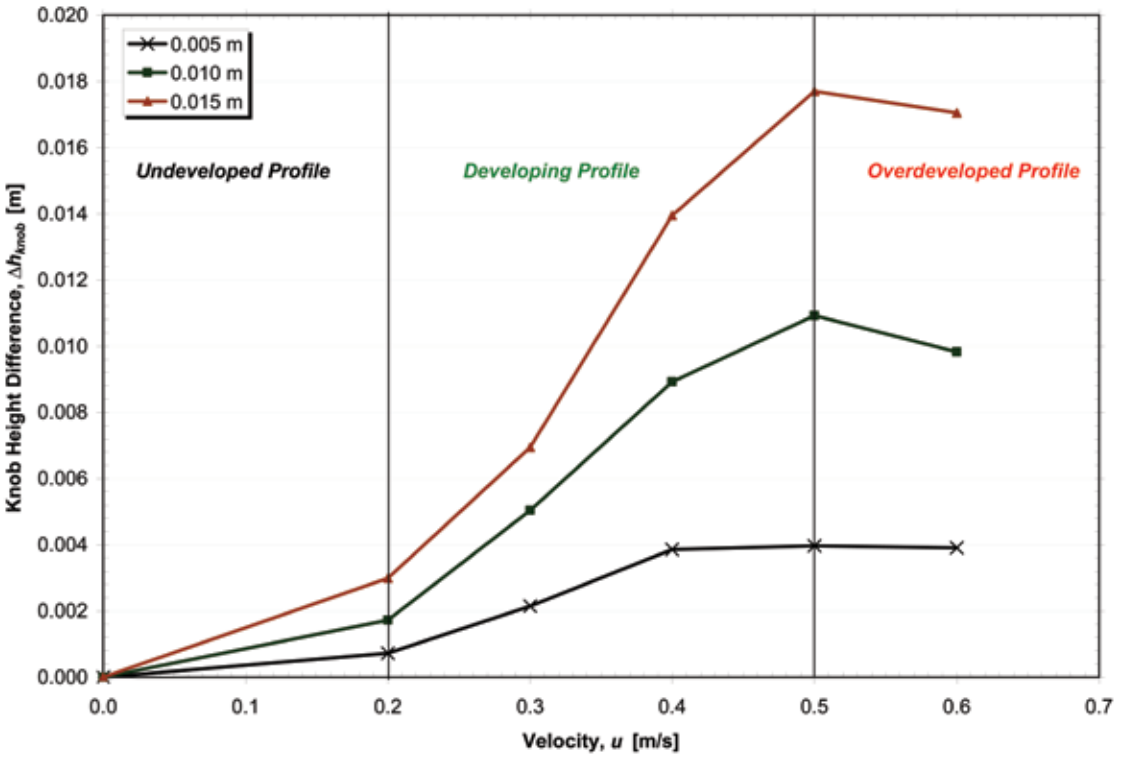

Relation between steel surface velocity and measured height of knob from nail board test (with slag).

is most sensitive to velocity in the important range of 0.2–0.5 m/second. Within this range, height difference increases with increasing surface velocity and increasing nail diameter. Excessive surface velocities lead to slag entrainment defects, while insufficient velocities lead to meniscus freezing and other defects. Single-roll and unstable flow patterns are inferior to a stable double-roll flow pattern with an optimized, intermediate surface flow velocity. These model results enable easier calibration/validation of computational models of fluid flow in the mold, in addition to helping nail board tests become a more powerful measurement tool.

Process Optimization With Offline Models

Process models are particularly useful when the phenomena of interest are very difficult to measure directly or to model physically. A good process model can be validated to match any measurements that are available, and then perform parametric studies to extrapolate the results to other locations and conditions, and help to find optimal windows of plant operation where product quality is best.

Mold Flow Control With Local Electromagnetic Braking — For example, fluid flow in a continuous casting mold can be controlled with electromagnetic forces, combined with other casting conditions, nozzle and mold geometry. Many previous computational models have been applied to this challenge.[22] The effects of varying electromagnetic braking (EMBr) field strength and SEN submergence depth on fluid flow in the mold cavity have been investigated with computational flow models, aided by plant measurements of field strength, surface shape and velocity.[23] Using the knowledge gained from the model and measurements together, electromagnetic forces and submergence depth can be controlled together to stabilize the fluid flow in the mold cavity and thereby minimize casting defects.

Magnetic field contours for a localized static EMBr field (0.355 T) were measured in an operating thin-slab caster at Nucor Steel in Decatur, Ala. This caster features a standard bifurcated 2-port SEN (Figure 15) and

Table 1

Casting and Simulation Conditions

Casting speed	3.3 m/min.
Mold width	1,374 mm
Mold thickness	90 mm
Meniscus level below top of mold	100 mm
Domain width	687 mm
Domain thickness	45 mm
Domain length	2,500 mm
ρ_{steel}	7,000 kg/m^3
ρ_{slag}	3,000 kg/m^3
μ	0.006 kg/m-s
σ	714,000 $(\Omega\text{-m})^{-1}$
Gravity	9.81 m/s^2

Figure 15

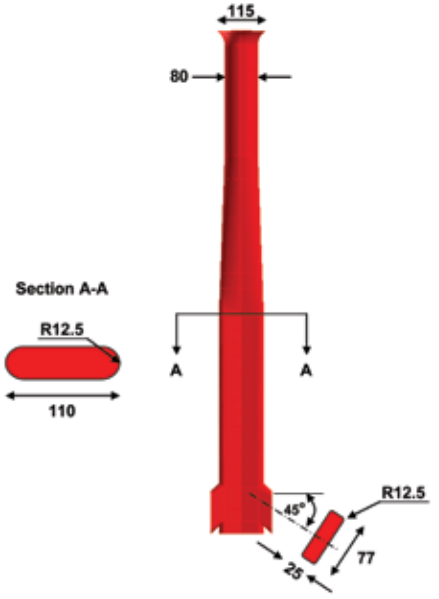

Nozzle geometry.

Figure 16

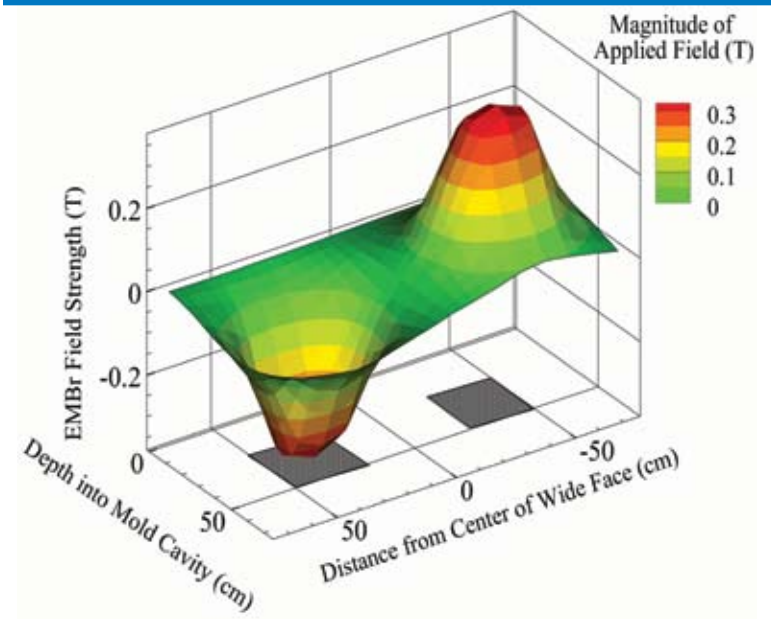

Measured electromagnetic field contours (0.355 T).

a 90-mm-thick, straight parallel mold. Table 1 gives the casting conditions. A gauss meter was used to measure the magnetic field strength in the center plane. A typical 3-D contour plot is given in Figure 16. The gray-hatched squares indicate the physical location of the magnets. The maximum strength of 0.32 T is centered in an oval region, which is typical of local braking. The contour levels scale well with overall field strength.

A standard Reynolds-averaged Navier-Stokes model of turbulent fluid flow, including electromagnetics, was used to simulate the time-averaged flow pattern in the 90-mm-thick slab-casting mold with local EMBr. The steady-state, incompressible, 3-D Navier-Stokes equations are solved in the nozzle and mold domain using the magnetic induction method for solving for electromagnetic force,[24] and the standard k-ε model in FLUENT.[24] The mold domain consists of the liquid pool with the solidifying shell modeled with mass and momentum sinks.[23] The nine cases given in Table 2 investigate the combined influences of SEN depth and field strength on the flow pattern. Attention is focused on the surface velocity profile, turbulence levels and surface level profile, which governs quality of the cast product. The surface level profile is calculated from the pressure field, based on a potential energy balance.[25]

Table 2

Parametric Study

	SEN depth (mm)	EMBr setting (T)
Case 1	250	0
Case 2	250	0.2525
Case 3	250	0.355
Case 4	300	0
Case 5	300	0.2525
Case 6	300	0.355
Case 7	350	0
Case 8	350	0.2525
Case 9	350	0.355

A typical computed flow pattern (Figure 17) shows velocity vectors on the wide-face center plane for Case 6. The jet exiting the nozzle travels across the mold cavity, impinges on the narrow face, splits into upward and downward jets, creating the classic upper and lower recirculation zones of a double-roll flow pattern. In the upper recirculation zone, fluid flows up the narrow face, back across the top surface, and down the SEN wall to rejoin the jet exiting the nozzle. The brake causes some of the secondary jet flowing up the narrow face to split off early and flow back across the mold just above the brake region, altering velocities in the upper recirculation region. The lower recirculation zone is much larger and has lower velocities than the upper zone, because it is not confined. The upper zone is constrained by the top surface and the jet exiting the SEN, which tends to bend the jet slightly upward.

Velocity across the top surface is compared for all nine cases in Figure 18, which shows velocity toward the SEN on a line across the wide-face center plane 10 mm below the meniscus. A parabolic velocity profile is seen, with a maximum about 450 mm from the mold center. Increasing EMBr field strength at constant SEN depth causes a steeper downward jet angle, lower velocities and a flatter meniscus profile. Without EMBr (and with constant field strength), surface velocity decreases with increasing SEN depth. With EMBr, this trend reverses, because the jet drops below the EMBr region and maintains its momentum. Further details are given elsewhere.

Figure 17

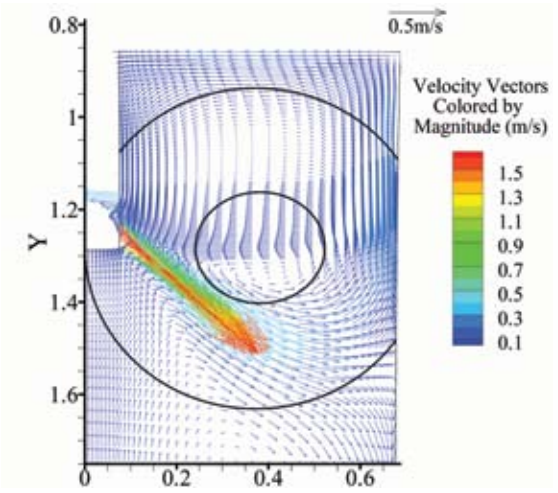

Velocity vectors on the mold wide face center plane for Case 6: outer circle shows extent of EMBr field, and inner circle shows region of strongest field.

Figure 18

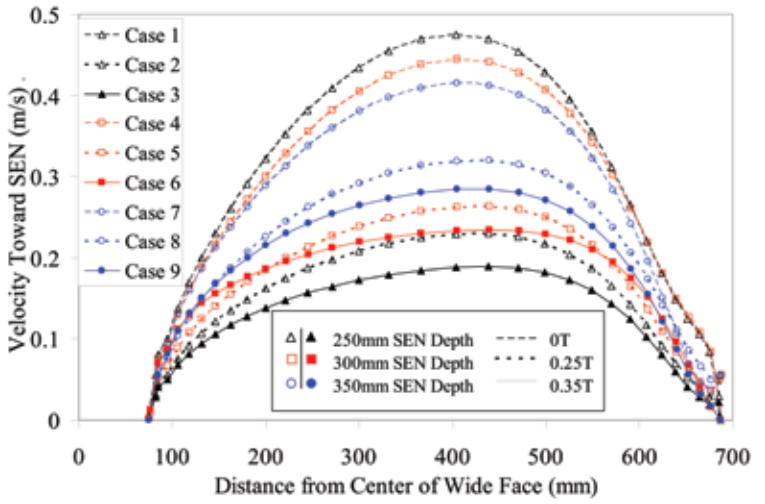

Velocity across top surface toward SEN for cases in Table 2.

After validating the model with a test problem, the results were validated by comparing with plant measurements of surface velocity from nail boards and meniscus shape (standing wave height) from oscillation mark profiles. Figure 19 compares the computed surface velocities with nail board test measurements using 10 nails, each 7.5 m long and 5 mm in diameter, converted to velocities using Figure 14. The numerical results match surprisingly well both near the narrow face and near the SEN.

The model was also validated by comparing the simulated shape of the top surface at the meniscus with oscillation mark profiles across the slab, as shown in Figure 20. Oscillation mark depressions reveal the shape of the meniscus at the instant in time they formed. The calculated profile roughly matches that measured from the photograph of the oscillation marks traced on a sand-blasted slab surface. Both show a high wave at the narrow face that slopes downward and stabilizes about halfway across the wide face before sloping slightly upward near the SEN. The average standing wave height of 4.41 mm compares well with the calculated average of 5.26 mm.

This parametric study provides insight into how to best operate this particular caster for these conditions. The local EMBr is beneficial, as it lowers surface velocity and flattens the meniscus profile (standing wave height). This prevents excessive surface velocities, and the corresponding slag entrainment, level fluctuations, inclusions and surface defects that accompany casting without electromagnetics for this geometry and casting speed. The EMBr field strength should vary with SEN depth to maintain constant meniscus conditions. Optimum operation depends on the location of the EMBr field relative to the SEN port outlets. For this caster, higher EMBr field strength is needed with deeper SEN submergence.

Figure 19

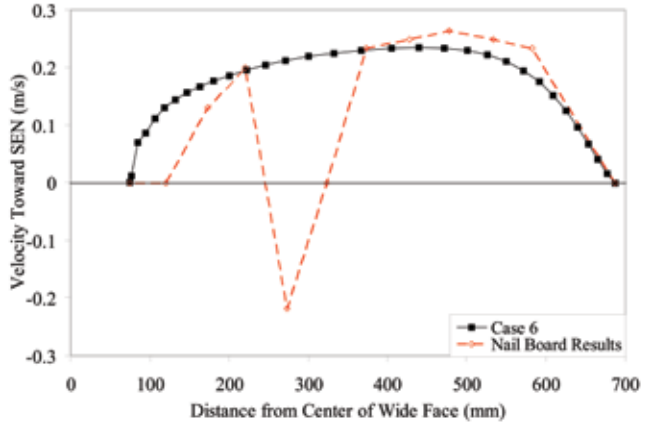

Comparison of calculated and experimental meniscus velocity.

Figure 20

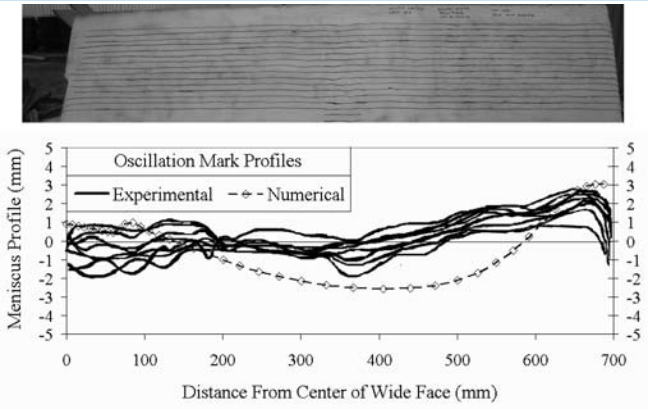

Comparison of calculated meniscus profile with oscillation marks (Case 6).

Figure 21

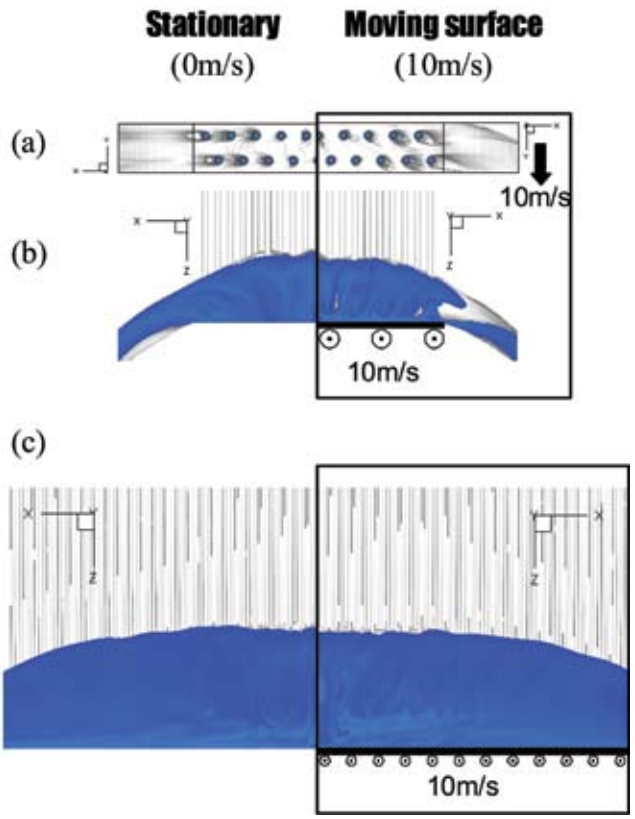

Water pool height comparison between stationary and moving surfaces: (a) 300-mm width (top view), (b) 300-mm width (front view) and (c) 1,200-mm width.

Figure 22

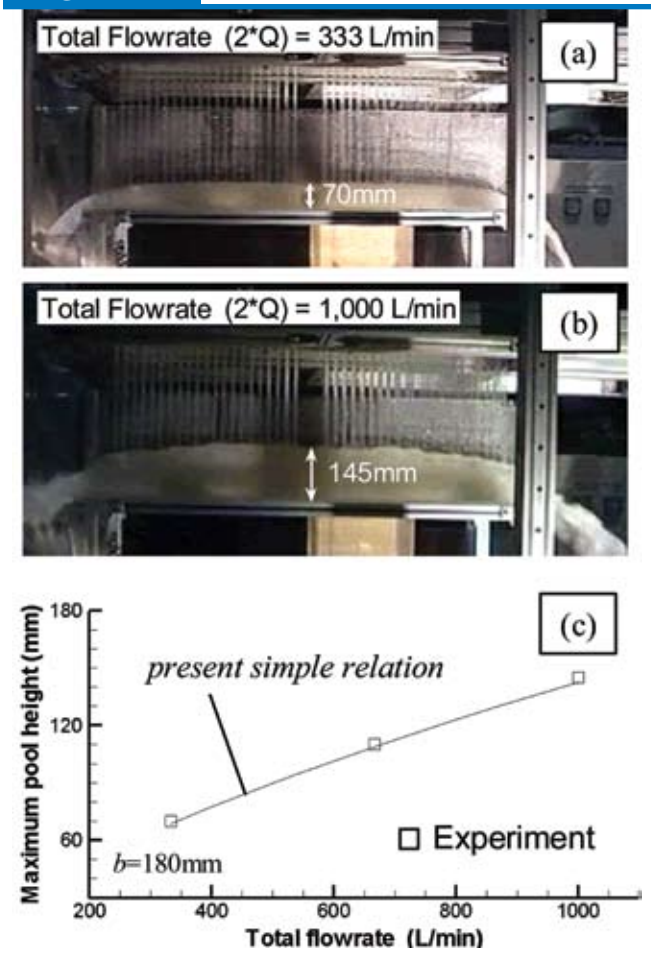

Comparison of water pool height.

Scale-Up From Lab Experiments to Plant Operation

Models are very useful in the design of new processes. Fundamentally based offline models can predict the differences between lab-scale experiments and full-scale plant operation, so long as they incorporate the relevant mechanistic phenomena. A model can help identify which process variables are most critical, or rate-limiting. Experiments can then focus on quantifying the effects of just these variables. Models can help ensure that the crucial phenomena which govern the real process are not overlooked.

Runout Table Cooling — Taking the downstream example of hot strip cooling on a runout table, lab experiments are needed to characterize the complex film-boiling phenomena that govern heat transfer between the cooling water and the hot steel strip.[26] The resulting heat transfer coefficients can then be used in online computational process models to control the water flowrates to achieve the desired cooling temperature. Accurate models of this process are especially important during the initial stages of open-loop model-based control, before the strip passes the optical pyrometers that enable true feedback-based control.

In performing the lab-scale experiments, it is obviously important to keep conditions as similar as possible to the full-scale plant operation. Thus, the same water nozzle geometry, water flowrates, strip temperatures, steel compositions and strip velocity should be used in the experiments as in the plant. Of course, lab experiments always have some unavoidable differences with the full-scale plant, which must be taken into account during scale-up. In this example, the size of the strip surface area and the number of nozzles are much smaller in the lab runout table. These differences have important consequences that might be overlooked, without the help of advanced computational models. Specifically, the greater surface area and the higher total water flow from the extra nozzles together make it more difficult for water to escape from the sides of the strip in the commercial operation. This causes the water level to build up, which in turn lessens the impact pressure on the strip. This causes lower heat transfer coefficients in the commercial operation, in spite of all other conditions being the same.

This behavior has been quantified with the use of a 3-D computational model of turbulent fluid flow in the runout table cooling process, including a volume of fluid (VOF) calculation of the free surface shape.[26] Figure 21 compares the water levels predicted across the strip width by the computational model in both the small, shallow, laboratory-scale model and the wide, deep, commercial operation. A water model constructed to investigate this aspect of the process, shown in Figure 22, confirms the accuracy of the computational

model. Parametric studies with this model have led to a simple relation to predict the water level (Figure 22c), thus facilitating more accurate scale-up to commercial operation. Further details on this modeling investigation can be found elsewhere[26] and in this proceedings.

Process Optimization With Semi-Online Models

Process models can be implemented very effectively when they run efficiently and deliver useful information to the plant operator as a semi-online model. The same model can also be applied by process engineers to optimize standard operating practices and other purposes. The key for success is that the model be accurate, fast and user-friendly. To be accurate, such models must be calibrated to match a few key plant measurements and/or a previously validated fundamental model. Then they can be applied to that specific plant to predict behavior for a specific set of operating conditions, or to perform parametric studies for optimization.

Selecting Order Sequences to Minimize Downgrading due to Grade Transitions — For example, a computational model of intermixing in the tundish and mold of a general continuous casting operation has been applied to predict and optimize casting conditions to minimize intermixing during grade changes.[27–28] The first step in predicting the extent of intermixing in the final product is to model the fluid flow pattern in tundish, and the corresponding transport of solute during a grade change when a new ladle opens. A great deal of previous work by many modelers has been done to understand and quantify fluid flow and the transport of heat, solute and inclusions in different tundish designs. These models have investigated the effect of tundish geometry, dams, weirs, impact pads, filters, bubble curtains, and other devices that control flow and transport. An important contribution of models, such as shown by Guthrie[29] and Sahai,[30] is that natural convection sometimes greatly changes the flow pattern. This effect becomes important and must be accounted for when the modified Froude number is large. Thus, transient flow through the tundish can change during a heat, as steel in the ladle cools and feeds colder, denser and heavier steel into the tundish. Similar changes in flow pattern occur due to the significant density differences between different steel grades (with the same superheat).

For example, Figures 23a and b compare the flow velocities predicted in a typical two-chambered tundish with different inlet temperatures using a 3-D model of turbulent flow coupled with heat transfer.[31] When tundish temperature is uniform, fluid exits the first chamber and travels along the bottom, quickly leaving the outlet. The top bulk of the tundish is almost stagnant, with a slow, counter-clockwise flow. However, when the inlet temperature is raised 5°C (from 1,548 to 1,553°C), the flow exiting the first chamber is hotter and less dense, so it rises quickly upon entering the second chamber. It flows in a clockwise pattern along the top surface and down the far wall, exiting the outlet with a longer residence path that is much better for floating out inclusions (Figure 23b). Figure 23c shows the corresponding temperature field, which reveals that a temperature difference of only a few degrees is enough to cause this complete reversal of the flow pattern.

Knowing the flow pattern, concentration in the tundish can be computed with an uncoupled solute transport model. For greater efficiency, concentration profiles leaving the tundish are computed with a simplified mixing model.[27] An example is shown in Figure 24, compared with plant measurements.

Figure 23

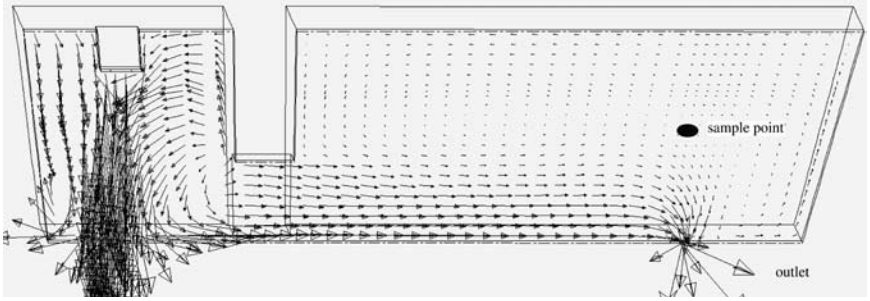

(a) Isothermal flow pattern (or high-carbon steel pouring into low-carbon steel)

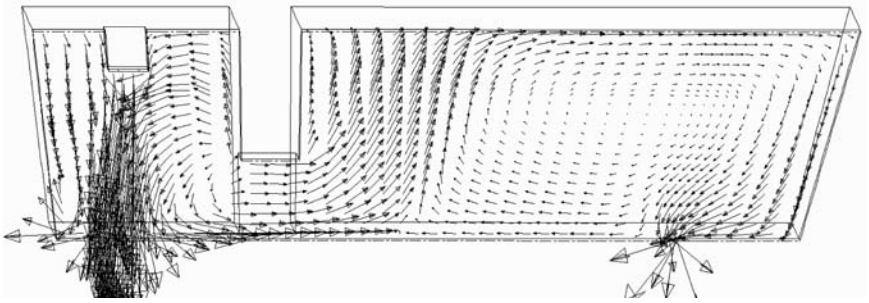

(b) Flow pattern for hot new steel flowing into a full tundish of 5°C cooler steel (or low-carbon steel pouring into high-carbon steel)

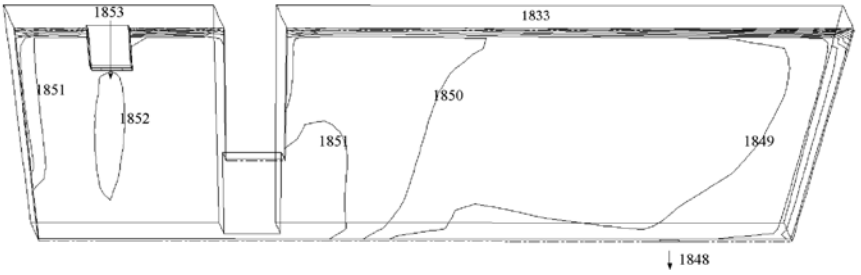

(c) Temperature distribution driving the flow pattern in (b)

Flow velocities predicted in a typical two-chambered tundish with different inlet temperatures.

Figure 24

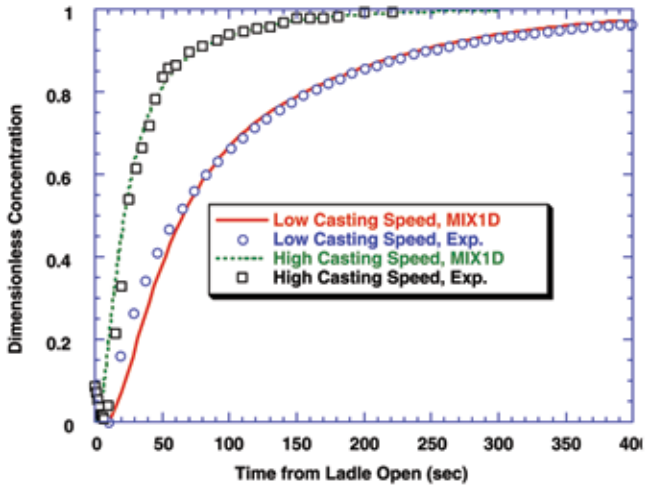

Concentration evolution from the tundish.

Figure 25

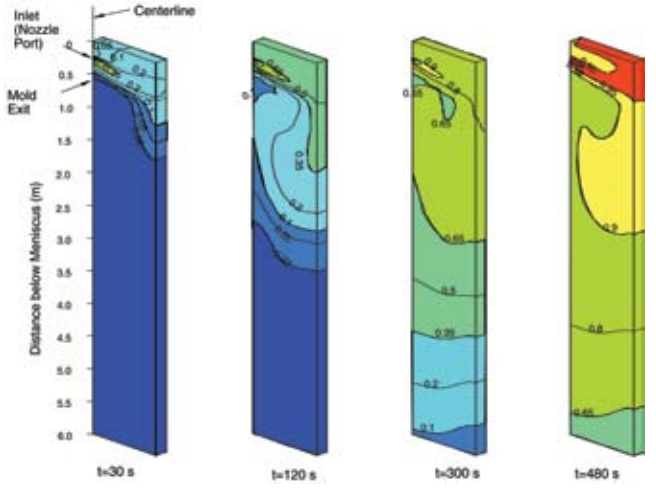

Concentration evolution in the strand.

Intermixing also depends on flow in the mold, especially when the minimum tundish weight during the grade change is small, and the strand section size is large.[27] Thus, similar 3-D computations of flow and solute transport in the mold have been performed. An example is given in Figure 25, casting red steel (C = 1) into blue steel (C = 0) for a flying tundish change (no tundish mixing). Note that solute penetrates deep into the strand faster than the casting speed. Combining these results with a model of shell growth, concentration profiles in the final product can be computed, knowing that diffusion in the solid is negligibly slow. Figure 26 shows an example, with distance along the slab reported relative to the meniscus location at the time of ladle opening. Note that the new grade penetrates deep into the center of the old slab (beyond +6 m), while the old grade persists on the surface of the new slab (beyond –6 m). Thus, plant measurements should focus on these two critical locations when resources are limited. Measurements over the entire length of the center and surface (Figure 27) confirm these predictions.

The next step is to develop a faster, simpler version of the models, in order to conduct many parametric studies and to provide an efficient semi-online model for plant operators. The complete 3-D models are very expensive, considering the fully transient nature of the lowering and raising of the tundish level during a typical transition. These simpler mixing box–based models are calibrated and validated with both the 3-D models and the plant measurements, as shown in Figure 27. To predict the locations along the strand where intermixing becomes excessive requires a search over all of the elements, knowing the compositions of both steel grades, and the customer specifications (composition tolerances) for each grade. A stringent grade can tolerate very little intermixing with the second grade, such as an ultralow-carbon steel cast before a high-carbon steel. A lenient grade, on the other hand, can tolerate a great deal of the other grade, such as two similar grades of rebar cast in a sequence. A user-friendly model, MIX1D, has been developed which incorporates all of the above functions.[32] It has been implemented as a semi-online model to predict intermixing in an operating bloom caster.

Figure 26

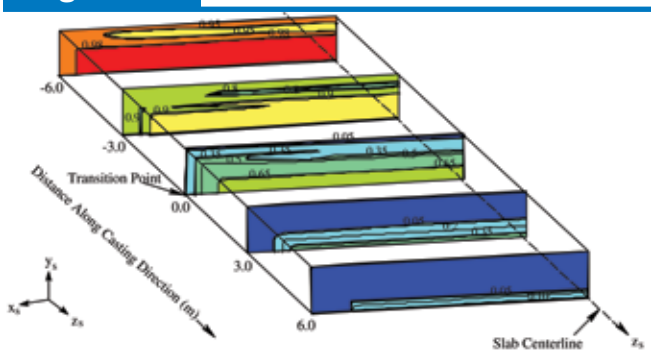

Composition distribution in the strand (3-D model).

Figure 27

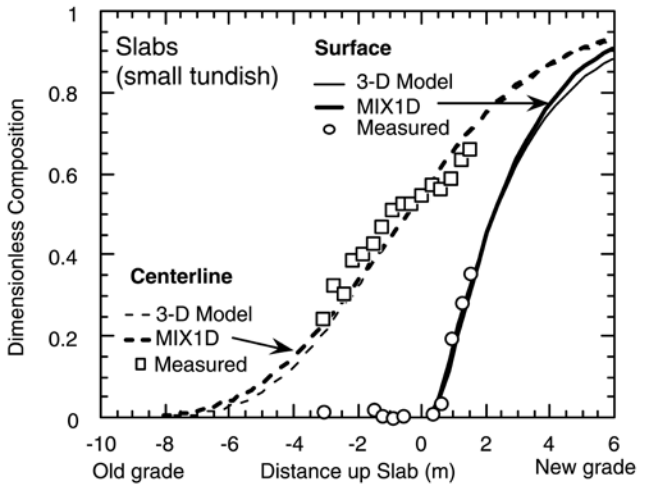

Composition distribution in the strand.

Figure 28

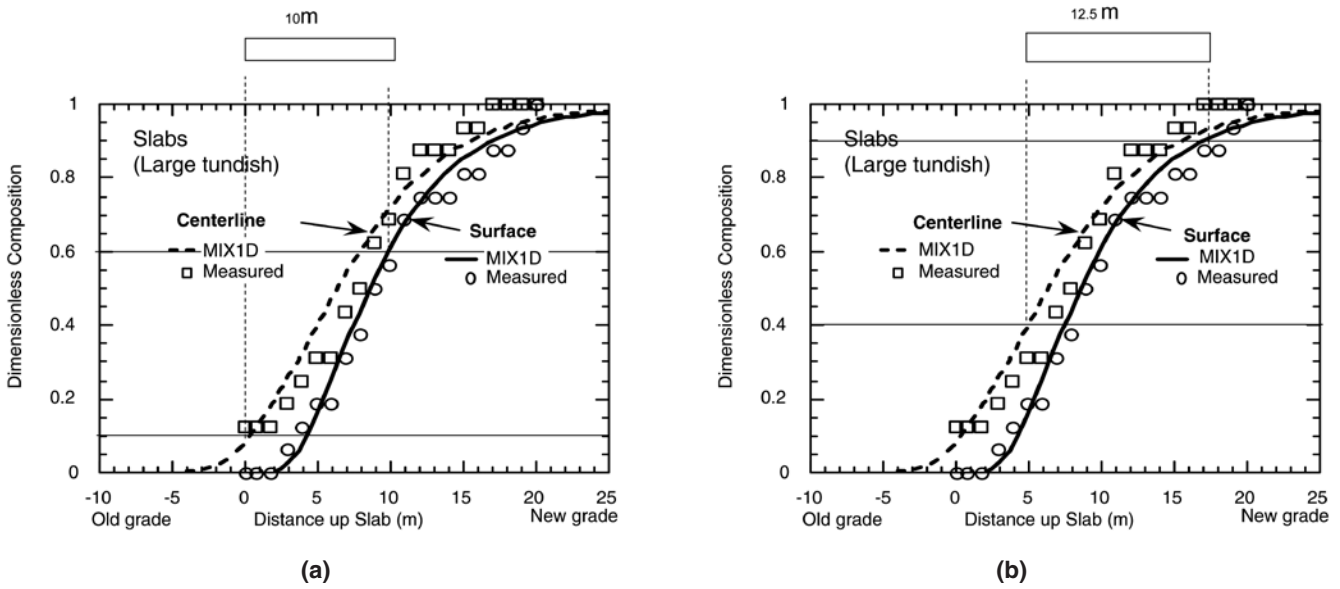

Computed location of slab to downgrade, for the same composition profiles with different grade specifications: (a) stringent to lenient transition (60–10) and (b) lenient to stringent transition (10–40).

Parametric studies with this efficient, simplified model provide both general guidelines for operation, as well as specific intermixing lengths for a given tundish and mold operation. Figure 28 shows an example, comparing the effect of the order when casting two steels with different tolerances. The stringent grade should be cast first when there is a large tundish with a lot of intermix.[28,33] For small tundishes where intermixing is dominated by the mixing in the strand, the order does not matter.

In general, the optimal casting conditions to minimize the intermix length for a stringent grade change are as follows: minimize mixing in the tundish, start to reduce casting speed long before ladle open, keep speed slow several minutes after ladle open, lower tundish weight at ladle open (the time prior to ladle open does not matter), hold tundish weight and speed constant for several minutes after ladle open, ramp speed and weight up to steady state slowly, and cast thin, narrow slabs if possible. In contrast, the optimal conditions for clean steel are: maintain a large-volume tundish, constant great depth (to minimize vortexing), flow control devices which maximize residence time and avoid short-circuiting, avoiding excessive turbulence at top surface, preventing reoxidation (with an optimal slag layer), and ensuring free-opening ladles (to avoid open pouring).

The results from this model can be used by process engineers to design standard practice during stringent grade changes, which will minimize the amount of steel that must be downgraded due to intermixing. When a downgrade market exists, traditional clean-steel practices can be applied to keep the intermixed steel in a single slab. Once calibrated for a particular operation, this simple model can be used by schedulers as an aid in optimizing sequence orders by quantifying the costs (in intermixed length) associated with casting dissimilar grades together. Sometimes, it is better to simply shut down the caster and start another sequence.

Finally, and most importantly, a rigorously calibrated version of this 1-D intermixing model has been used as a semi-online model by operators to indicate the optimum places to cut the strand during grade change operations, in order to minimize the amount of intermixed steel that must be downgraded.[27,32]

Real-Time Process Control

Finally, online computational models are increasingly able to implement beneficial changes into process operation on a continuous basis, as part of online control systems. Fully online models make adjustments to the process directly, without the need for operator interaction. As computers become faster, however, increasingly advanced computational models can run in real time. This is enabling more sophisticated, mechanistic, model-based control systems.

Secondary Spray Cooling — A recent example of online model-based control systems is found in the control of secondary cooling in continuous slab casting operations.[34–35] Secondary cooling presents several challenges to control. The first challenge is to find water flowrates that maintain a reasonable temperature profile down the caster during steady-state casting. With non-optimal cooling, surface cracks can form due to thermal stresses caused by overcooling and subsequent reheating, or by bending or unbending while the steel surface is in a temperature region of low ductility. In general, less cooling is needed at lower casting speed, owing to the inherent extra cooling time. However, defects will result on any portion of the strand that is overcooled or undercooled, regardless of speed. Modern air-mist cooling nozzles offer the potential advantage of more uniform cooling, but introduce the extra challenge of air flowrate as another process variable to control.

Once reasonable steady-state water and air flowrates are found for each spray zone and casting speed, many operations use simple “look-up” tables to change these

Figure 29

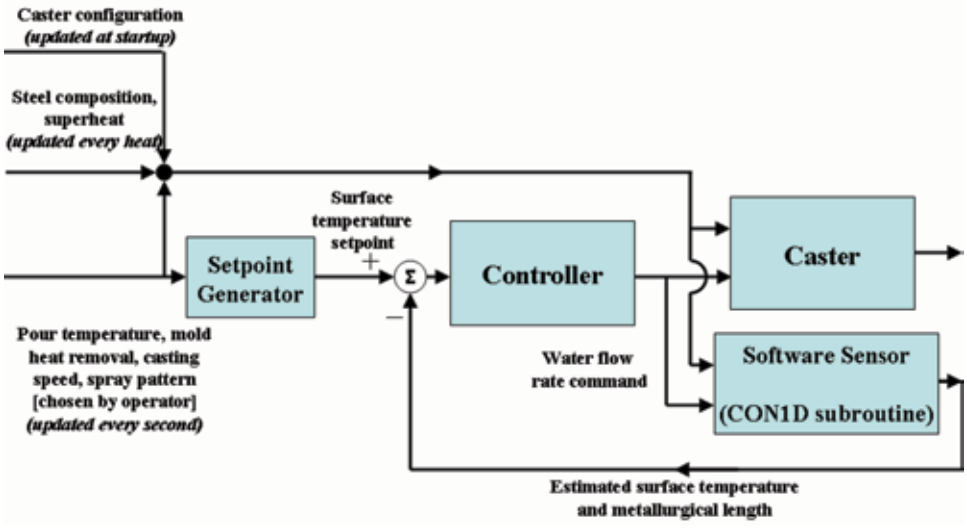

(a)

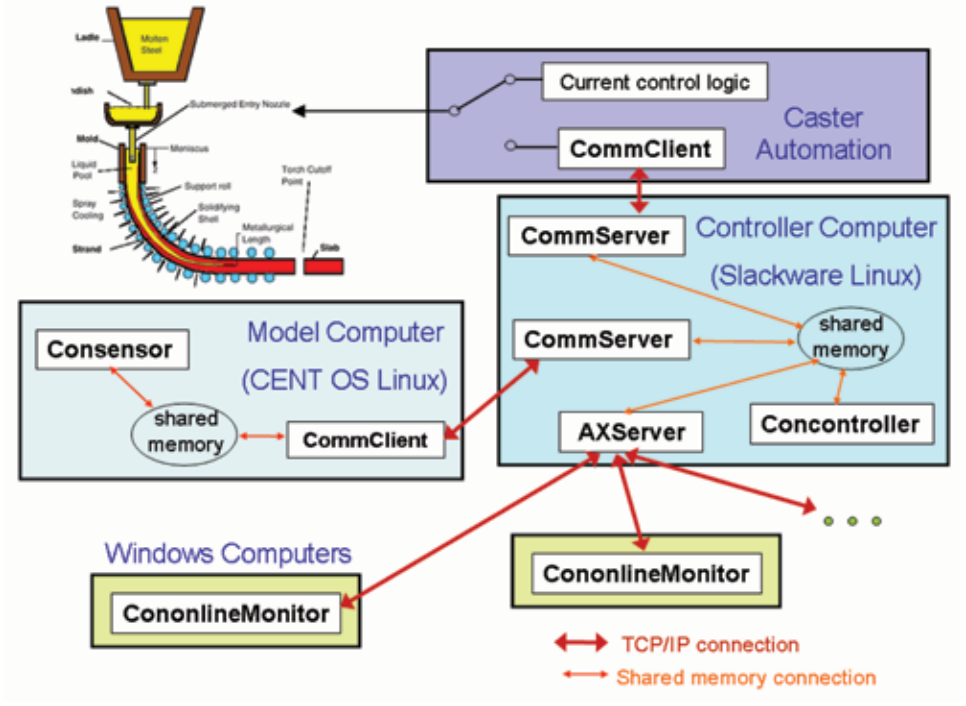

(b)

Software sensor–based control system: (a) flow diagram and (b) hardware and software.

flowrates automatically according to the current casting speed. However, the heat content and thermal resistance of the solid shell increases down the caster. This causes slower thermal response dynamics with distance down the caster during speed changes. A dynamic spray cooling system is needed to take this into account, and to adjust each spray flowrate to maintain the same thermal history for each portion of the strand.

Conventional feedback control systems based on hardware sensors have never been successful because emissivity variations from intermittent surface scale and the harsh environment of the steam-filled spray chamber make optical pyrometers unreliable. Recently, computational models have been used as "software sensors" to predict the transient temperature distribution of the entire strand in real time, and to feed those predictions into a controller.

The models in these control systems are essentially versions of the one-dimensional finite-difference models used by the early modeling pioneers such as Brimacombe and discussed previously. The extra challenge is to simulate the entire temperature history of the strand (not just one slice), and to accomplish this in real time. Previous online dynamic models have been applied to control the spray cooling of thick slab-casters, including Hardin et al.[36] at IPSCO (now SSAB), Iowa, and Leehuenkilpi and coworkers using DYNCOOL at Rautaruukki Oy Raahe Steel Works,[37] and other unpublished models.

One such model-based control system has been developed recently at the University of Illinois in collaboration with Nucor Steel in Decatur, Ala. It is being applied to control secondary cooling in their thin-slab casting operation, where the high casting speeds require robust execution of the entire model and control system with prediction updates every second. The control system is shown schematically in Figure 29.

The core of the system is a software sensor based on the model CON1D.[38] CON1D is a simple but comprehensive, fundamentally based model of heat transfer and solidification of the continuous casting of steel slabs, including phenomena in both the mold and the spray regions. The accuracy of this model in predicting heat transfer and solidification has been demonstrated through comparison with analytical solutions and plant measurements, both in the mold and below.[38] The simulation domain of CON1D is a transverse slice through the strand thickness that spans from the center of the shell surface of the inner radius to that of the outer radius. This model computes the temperature and solidification history of each slice as it traverses the path from the meniscus down through the spray zones to the end of the caster, as shown in Figure 30. It features a detailed treatment of the spray region, including the variation in heat transfer

Figure 30

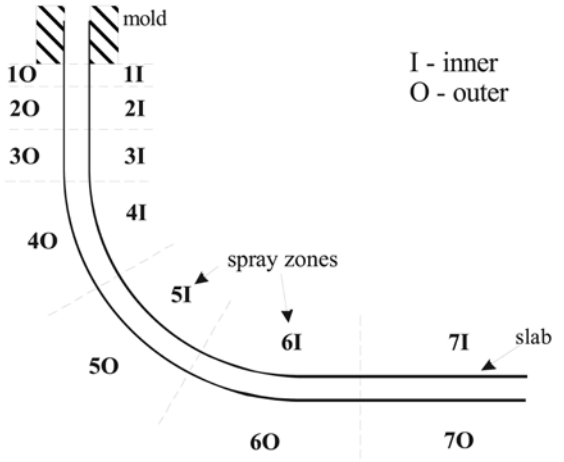

Simulation zones of the model domain from mold to cutoff shear.

Figure 31

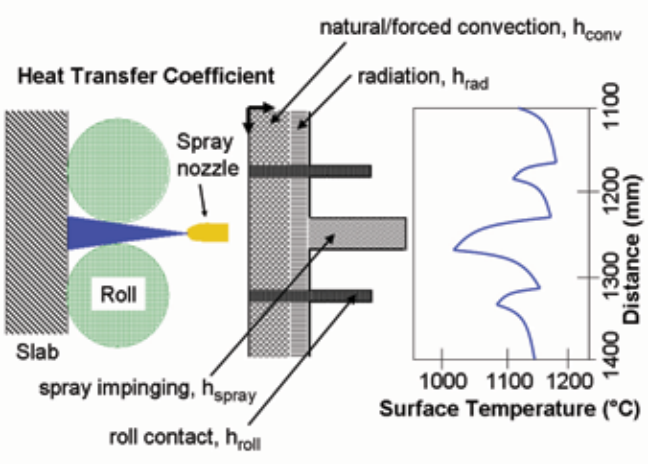

Schematic of spray zone region, heat transfer coefficients, and corresponding surface temperature variations.

coefficients as the strand passes between individual rolls and under each row of spray nozzles. The model simulates the temperature drops due to heat extraction to each individual roll and by the water sprays in between, as shown in Figure 31. Notice the pattern of temperature peaks and dips. The temperature dips are caused by water spray impingement and roll contact, whereas the temperature peaks occur where convection and radiation are the only mechanisms of heat extraction. To achieve the complete transient history of the entire strand, the software sensor, CONONLINE, manages multiple slices and their respective temperature histories, and interpolates between them. It uses CON1D as a sub-routine to compute each slice. More detail is given elsewhere.[34–35]

Figure 32

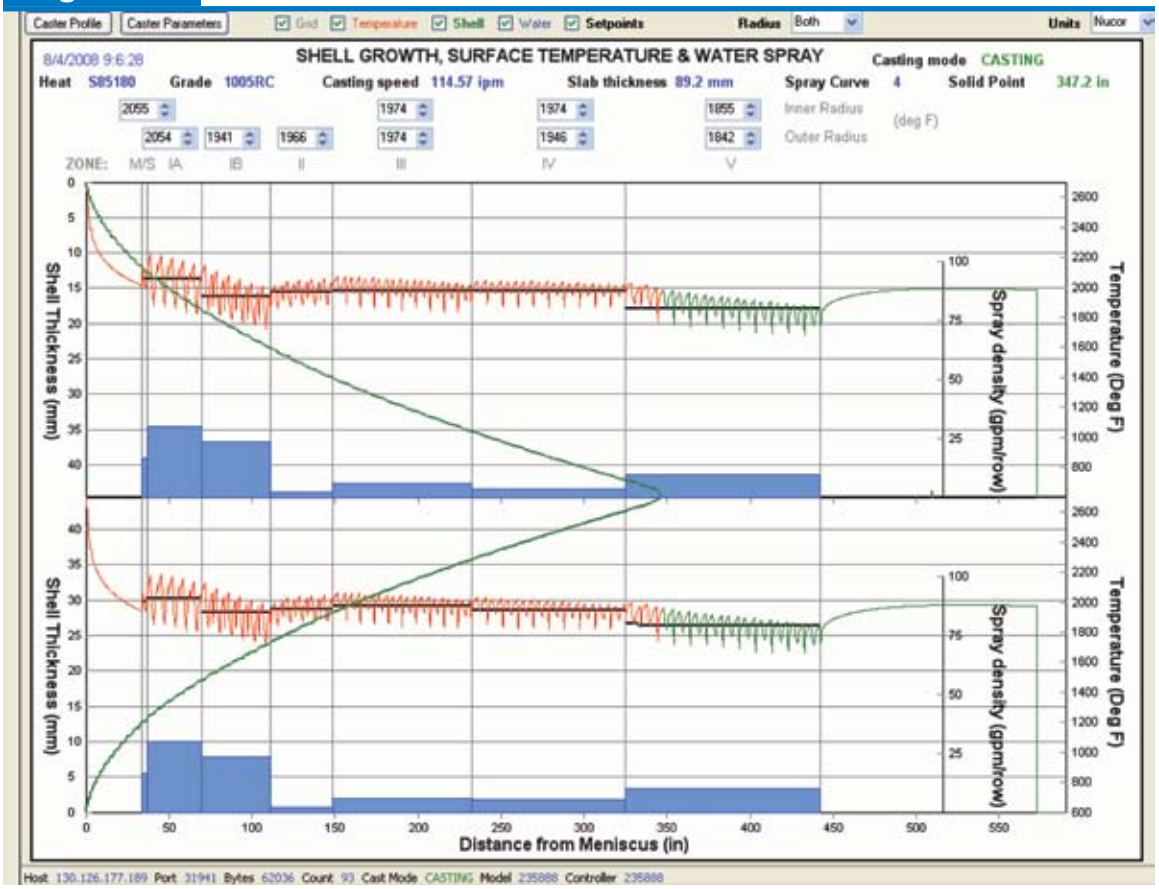

Real-time monitor interface, displaying shell thickness profile, surface temperatures, setpoints, flowrates, etc.

The purpose of the software sensor is to provide a real-time estimate of the temperature of the entire outer surface of the steel strand, based on all available casting conditions. This is the same function that temperature sensors would perform in a traditional feedback control system. The predicted shell temperature profile is averaged over each zone and compared against a preset profile of surface temperature profile setpoints (Figure 30). The setpoints are selected from a database of standard operating practices that can be altered by the operator, and smoothed by the setpoint generator. The mismatch between the predicted temperatures and the setpoints is sent to the controller to compute the water flowrates required to drive the mismatch to zero. These computed flowrates are sent to both the operating caster and back to the software sensor to begin the loop again for the next time interval.

The system hardware (Figure 31) features separate computers for the software sensor and the controller, connected through shared memory with the level 2 control system at the caster. Operators interact with the system through a monitor on the casting pulpit desktop Windows computers. A screenshot is given in Figure 32. This real-time interface displays on both the inside and outside radii: the predicted shell thickness profile, shell surface temperature, the zone-averaged temperature setpoints, the current spray-water flowrates and other information. In addition, operators can input new setpoints through this interface.

By presenting accurate information to the operator in real time in a natural visual manner, this system empowers the operator to react better to unforeseen situations. In addition to controlling surface temperature, another important objective of the system is to avoid costly and dangerous "whale" formation. A whale forms when the metallurgical length extends past the last set of support rolls, and the internal ferrostatic pressure causes excessive bulging of the strand. While this system was being tested on the North caster, prior to giving it full automatic control, operators watching the monitor were able to recognize impending problems and avoided whale formation. The South caster, which did not have the system, experienced a whale during this time. Ultimately, a truly "expert" caster control system should recognize and take appropriate action to prevent these and other problems, in addition to controlling sprays to maintain surface temperature.

Conclusions

This paper has offered a few examples of the different ways in which computational models can be applied to implement beneficial change to steel processing. These include fully online models, semi-online models, offline models and literature models. Process models range from empirical to mechanistic in nature and vary in complexity from simple analytical solutions to coupled, 3-D transient numerical simulations. Advances in computing have enabled tremendous increases in the power of models over the years.

I am humbled by the wisdom of early pioneers such as Harry Howe, who were able to understand so much using only their wits and powers of observation, while lacking such basic tools as the phase diagram and the computer. Later pioneers, such as Keith Brimacombe, taught us how to develop mathematical models, validate them with experiments and plant trials, and apply them to gain insight and solve practical problems. They remind us that future advances will not come from either models, experiments or plant trials; they will come from ideas generated by people who understand the process and the problems.

Acknowledgments

I wish to thank the member companies of the Continuous Casting Consortium, and the National Science Foundation for over two decades of support, the National Center for Supercomputing Applications for computational resources, and my mentors, which include Keith Brimacombe. But most of all, I thank my graduate students and visitors to my lab who did so much dedicated, hard work on these modeling projects over the past two decades, including: Avijit Moitra, Guowei Li, Hong Zhu, Hua Bai, Jun-Kil Park, Ya Meng, Quan Yuan, Chunsheng Li, Seid Koric, Jorg Peter, Ho-Jung Shin, Kun Xu, Bryan Petrus, Sami Vahpalahti, Matt Rowan, Rui Liu, Maria-Rita Ridolfi, Rodrigo Marin, Guowei Li, Xiaoqing Huang, Mustapha El-Bealy, Yuji Miki, Martin Fackeldey, Young-Mok Won, Kuan-Ju Lin, Lifeng Zhang, Joydeep Sengupta, Ho-Jung Shin, Seon-Hyo Kim, Dianfeng Li, Go-Gi Lee, Claudio Ojeda, S. Louhenkilpi, Claudia Pfeiler, Prasanna Kumar, Ruan Xiaoming, Myung-Jong Cho, Seong-Mook Cho, Seong-Yeon Kim, Chengbin Li, Larry J. Mika, Jean A. Azzi, Glen T. Haegele, David D. Goettsch, William R. Storkman, Fady M. Najjar, Patrick F. Kozlowski, Bryant Ho, Donald E. Hershey, Robert M. McDavid, David T. Lui, Keith Rackers, David Creech, Sivaraj Sivaramakrishnan, Jon Parkman, Lan Yu, David T. Stone, Melody Langeneckert, Shanker Subramanian, Tiebio Shi, Joe Shaver, Bin Zhao, Jun Aoki, Sana Mahmood, Bret Rietow, Aravind Sundararajan, Michael Okelman, Kevin Cukierski, Lance Hibbeler, Rajneesh Chaudhary, Xiaoxu Zhou, Choul-Hong Min and Varun Singh.

References

1. H.M. Howe, "What Is Steel?" *Eng. and Mining J.*, Aug. 28 and Sept. 4, 11, 18, 1875.

2. B. Thomas and J.K. Brimacombe, "Process Modeling," Chap. 8, *Advanced Physical Chemistry in Process Metallurgy*, N. Sano, W. Lu and P. Riboud, eds., Academic Press, London, U.K., pp. 253–279, 1997.

3. O.C. Zienkiewicz and Y.K. Cheung, *The Finite Element Method in Structural and Continuum Mechanics,* McGraw-Hill Publishing Co., 1967.

4. E.A. Mizikar, "Mathematical Heat Transfer Model for Solidification of Continuously Cast Steel Slabs," *Trans. TMS-AIME,* 239, 11, pp. 1747–1753, 1967.

5. J.E. Lait, J.K. Brimacombe and F. Weinberg, "Mathematical Modelling of Heat Flow in the Continuous Casting of Steel," *Ironmaking and Steelmaking,* 1, 2, pp. 90–97, 1974.

6. J.E. Lait, J.K. Brimacombe, F. Weinberg and F.C. Muttitt, "The Liquid Pool Geometry and Cast Structure in Continuously Cast Blooms and Beam Blanks at the Algoma Steel Corp.," *Open Hearth Conf. Proc.,* 56, ISS, Warrendale, Pa., Cleveland, Ohio, pp. 269–302, 1973.

7. A.W.D. Hills, *J. of the Iron & Steel Institute,* 203, 18, 1965.

8. J.K. Brimacombe, "Design of Continuous Casting Machines Based on a Heat-Flow Analysis: State-of-the-Art Review," *Canadian Metall. Quart.,* 15, 2, pp. 163–175, 1976.

9. V.R. Voller and F. Porte-Agel, "Moore's Law and Numerical Modeling," *J. Computational Physics,* 179, pp. 1–6, 2002.

10. T. Brandvik and G. Pullan, "Acceleration of a 3-D Euler Solver Using Commodity Graphics Hardware," *46th AIAA Aerospace Sciences Meeting,* Reno, Nev., Jan. 2008.

11. T. Emi, "Theoretical and Process Study on Steelmaking and Steel Refining," *8th China Steelmaking Conference Proceedings,* China Metal Society, Beijing, China, pp. 8–10, 1994.

12. Y.Y. Sheng and G.A. Irons, "Turbulence Modeling of Plume Flows in a Gas Stirred Ladle," *Process Technology Conference Proceedings,* 10, ISS, Warrendale, Pa., pp. 143–150, 1992.

13. S.T. Johansen and F. Boysan, "Fluid Dynamics in Bubble Stirred Ladles: Part II, Mathematical Modeling," *Metall. Trans.,* 19B, pp. 755–764, 1988.

14. L. Zhang and F. Oeters, "Mathematical Modeling of Alloy Melting in Steel Melts," *Steel Research,* 70, 4–5, pp. 128–134, 1999.

15. D. Mazumdar and R.I.L. Guthrie, "Hydraudynamic Modeling of Some Gas Injection Processes in Ladle Metallurgy Operations," *Metall. Trans.,* 16B, pp. 83–90, 1985.

16. A.H. Castillejos and J.K. Brimacombe, "Measurements of Physical Characteristics of Bubbles in Gas-Liquid Plumes: Part II, Local Properties of Turbulent Air-Water Plumes in Vertically Injected Jets," *Metall. Trans.,* 18B, pp. 659–671, 1987.

17. J. Aoki, B.G. Thomas, J. Peter and K.D. Peaslee, "Experimental and Theoretical Investigation of Mixing in a Bottom Gas-Stirred Ladle," *AISTech 2004 Conference Proceedings,* pp. 1045–1056.

18. E.T. Turkdogan, *Fundamentals of Steelmaking,* London: The Institute of Materials, 1996.

19. P.H. Dauby, W.H. Emling and R. Sobolewski, "Lubrication in the Mold: A Multiple Variable System," *Ironmaker and Steelmaker,* 13, Feb, pp. 28–36, 1986.

20. B. Rietow and B.G. Thomas, "Using Nail Board Experiments to Quantify Surface Velocity in the CC Mold," *AISTech 2008 Conference Proceedings.*

21. M.S. Engleman, *FIDAP Theoretical Manual,* Fluent Inc., Evanston, Ill., 2001.

22. B.G. Thomas and L. Zhang, "Review: Mathematical Modeling of Fluid Flow in Continuous Casting," *ISIJ Internat.,* 41, 10, pp. 1181–1193, 2001.

23. K. Cukierski and B.G. Thomas, "Flow Control With Local Electromagnetic Braking in Continuous Casting of Steel Slabs," *Metals and Materials Transactions B,* 39B, 1, pp. 94–107, 2008.

24. FLUENT6.2-Manual, Ansys Inc., Lebanon, N.H.

25. Q. Yuan, B.G. Thomas and S.P. Vanka, "Study of Transient Flow and Particle Transport During Continuous Casting of Steel Slabs, Part 1, Fluid Flow," *Metal. & Material Trans. B.,* 35B, 4, pp. 685–702, 2004.

26. M.J. Cho, B.G. Thomas, and P.J. Lee, "3-D Numerical Study of Impinging Water Jets in Runout Table Cooling Processes," *Metals and Materials Transactions B,* 39B, pp. 593–602, 2008.

27. X. Huang and B.G. Thomas, "Intermixing Model of Continuous Casting During a Grade Transition," *Metall. Trans. B,* 27B, 4, 617–632, 1996.

28. B.G. Thomas, "Modeling Study of Intermixing in Tundish and Strand During a Continuous-Casting Grade Transition," *Iron and Steelmaker,* 24, 12, pp. 83–96, 1997.

29. S. Joo, R.I.L. Guthrie and C.J. Dobson, "Modelling of Heat Transfer, Fluid Flow and Inclusion Flotation in Tundishes," *Steelmaking Conf. Proc.,* 72, ISS, Warrendale, Pa., pp. 401–408, 1989.

30. C. Damle and Y. Sahai, "A Criterion for Water Modeling of Non-Isothermal Melt Flows in Continuous Casting Tundishes," *ISIJ Inter.,* 36, 6, pp. 681–689, 1996.

31. Y. Miki and B.G. Thomas, "Modeling of Inclusion Removal in a Tundish," *Metall. Mater. Trans. B,* 30B, 4, pp. 639–654, 1999.

32. B.G. Thomas and X. Huang, "MIX1D — Intermixing Model of Continuous Casting During a Grade Transition," Mechanical and Industrial Engineering, Univ. of Illinois, Urbana, Ill., 1994.

33. H. Chen and R.D. Pehlke, "Minimization of Transition Slabs Based on Tundish Flow Control," *Steelmaking Conf. Proc.,* 77, ISS, Warrendale, Pa., Chicago, Ill., pp. 695–702, 1994.

34. K. Zheng, B. Petrus, B.G. Thomas and J. Bentsman, "Design and Implementation of a Real-Time Spray Cooling Control System for Continuous Casting of Thin Steel Slabs," *AISTech 2007 Conference Proceedings*.

35. B.G. Thomas, J. Bentsman and K. Zheng, "Cooling Control System for Continuous Casting of Metal," U.S Nonprovisional Patent Application # TF07019, 2008.

36. R.A. Hardin, K. Liu, A. Kapoor and C. Beckermann, "A Transient Simulation and Dynamic Spray Cooling Control Model for Continuous Steel Casting," *Metal. & Material Trans.,* 34B, June, pp. 297–306, 2003.

37. M. Jauhola, et al., "Dynamic Secondary Cooling Model for a Continuous Casting Machine," *6th International Rolling Conference,* 1, Verein Deutscher Eisenhuttenleute, Düsseldorf, Germany, 20–22 June 1994, pp. 196–200.

38. Y. Meng and B.G. Thomas, "Heat Transfer and Solidification Model of Continuous Slab Casting: CON1D," *Metal. & Material Trans.,* 34B, 5, pp. 685–705, 2003. ✦

This paper was originally presented as the Howe Memorial Lecture at AISTech 2009 — The Iron & Steel Technology Conference and Exposition, St. Louis, Mo., and published in the Conference Proceedings.

Did you find this article to be of significant relevance to the advancement of steel technology?
If so, please consider nominating it for the AIST Hunt-Kelly Outstanding Paper Award at www.AIST.org/huntkelly.